The Astronomical Journal, 138:502–509, 2009 August doi:10.1088/0004-6256/138/2/502

AN OPTICAL AND X-RAY STUDY OF THE FOSSIL GROUP RX J1340.6+4018*

Claudia L. Mendes de Oliveira[1], Eduardo S. Cypriano[1,2], Renato A. Dupke[3,4], and Laerte Sodré Jr.[1]
[1] Departamento de Astronomia, Instituto de Astronomia, Geofísica e Ciências Atmosféricas da USP, Rua do Matão 1226, Cidade Universitária, 05508-090, São Paulo, Brazil; oliveira@astro.iag.usp.br, laerte@astro.iag.usp.br, cypriano@astro.iag.usp.br
[2] Department of Physics & Astronomy, University College London, London WC1E 6BT, UK
[3] University of Michigan, Ann Arbor, MI 48109, USA
[4] Observatório Nacional, Rua Gal. José Cristino 77, São Cristóvão, CEP20921-400 Rio de Janeiro RJ, Brazil; rdupke@umich.edu
Received 2008 February 24; accepted 2009 April 3; published 2009 June 30

ABSTRACT

Fossil groups are systems with one single central elliptical galaxy and an unusual lack of luminous galaxies in the inner regions. The standard explanation for the formation of these systems suggests that the lack of bright galaxies is due to galactic cannibalism. In this study, we show the results of an optical and X-ray analysis of RX J1340.6+4018, the prototype fossil group. The data indicate that RX J1340.6+4018 is similar to clusters in almost every sense (dynamical mass, X-ray luminosity, M/L, and luminosity function) except for the lack of L* galaxies. There are claims in the literature that fossil systems have a lack of small mass halos, compared to predictions based on the lambda cold dark matter scenario. The observational data gathered on this and other fossil groups so far offer no support for this idea. Analysis of the SN Ia/SN II ejecta ratio in the inner and outer regions shows a marginally significant central dominance of SN Ia material. This suggests that either the merger which originated in the central galaxy was dry or the group has been formed at early epochs, although better data are needed to confirm this result.

Key words: cooling flows – cosmology: observations – galaxies: clusters: individual (RXJ1340.6+4018, RXJ1552.2+2013, RXJ1416.4+2315) – galaxies: elliptical and lenticular, cD – galaxies: evolution – galaxies: kinematics and dynamics – galaxies: luminosity function, mass function – intergalactic medium

Online-only material: color figures

1. INTRODUCTION

Fossil groups (FGs) are bright and extended X-ray emission systems $\left(L_{X,\mathrm{bol}} > 10^{42}\ \mathrm{h}_{50}^{-2}\,\mathrm{erg\,s^{-1}}\right)$ dominated by a single giant elliptical galaxy and with at least a 2 mag difference between the first- and second-ranked galaxies (in the *R* band) within half of its virial radius. Initially, FGs were thought to be the cannibalistic remains of small galaxy groups that lost energy through tidal friction, perhaps the final stage of compact groups (e.g., Barnes 1989; Ponman & Bertram 1993; Jones et al. 2003). More recently, X-ray measurements of FGs were shown to be inconsistent with this formation mechanism, in particular because the intergalactic medium of a number of FGs is similar to those of galaxy clusters, with temperatures sometimes in excess of 4 keV (e.g., Khosroshahi et al. 2006; Khosroshahi et al. 2007) and, thus, FGs have high gravitational masses compared with most nearby groups. As an example, one of the most massive Hickson compact groups known, HCG 62, is an order of magnitude less massive than the typical FGs studied so far (Mendes de Oliveira & Carrasco 2007).

The high masses of FGs estimated in X-rays were confirmed by the dynamical studies of these systems. Recent measurements of galaxy velocity dispersions in FGs (Mendes de Oliveira et al. 2006; Cypriano et al. 2006; Khosroshahi et al. 2007) are fully consistent with the dynamical state of the system as determined from X-ray observations, indicating that they have relatively deep gravitational potential wells, typical of clusters.

The lack of L* galaxies in the central regions in a *cluster-sized* potential was quite intriguing at first and motivated a number of studies. D'Onghia et al. (2005) and Dariush et al. (2007) suggested that these systems are older than clusters of comparable masses. von Benda Beckmann et al. (2008), from the analysis of the magnitude gap between the brightest and the second most bright group member in a cosmological simulation, also suggest that fossil groups are old structures and point out that they are a transitory phase in the life of a group which ends with the infall of new galaxies from the neighborhood. Díaz-Giménez et al. (2008) analyzed FGs in the Millennium simulation (Springel et al. 2005) and in a mock catalog and concluded that although FGs have assembled early, first-ranked galaxies in FGs only formed their magnitude gaps and their luminous galaxies quite recently.

The most likely mechanism proposed for the lack of luminous galaxies surrounding the central dominant galaxy is cannibalism (e.g., Jones et al. 2003). The central merging, if not completely "dry" (i.e., involving gas-poor galaxies), should be accompanied by star formation bursts, causing subsequent metal-rich SN II-driven galactic winds or superwinds (e.g., Sanders & Mirabel 1996). These secular winds would deposit metals and energy into the central gas and this extra energy may contribute to explain the typical lack of cooling cores in FGs (Sun et al. 2004; Khosroshahi et al. 2004, 2007). The wind metal injection would make the central SN Ia/SN II ejecta of FGs different (lower) from that of normal groups and similar sized clusters. This scenario can, in principle, be tested by measuring individual elemental abundances and their ratios with sufficiently high signal-to-noise ratio (S/N) X-ray data (Dupke et al. 2009).

Based on the luminosity function of the fossil group RX J1340.6+4018 published by Jones et al. (2000) and on the conclusion that RX J1340.6+4018 lived in a sparse environment

* Based on observations obtained at the Gemini Observatory, which is operated by the Association of Universities for Research in Astronomy, Inc., under a cooperative agreement with the NSF on behalf of the Gemini partnership: the National Science Foundation (US), the Science and Technology Facilities Council (UK), the National Research Council (Canada), CONICYT (Chile), the Australian Research Council (Australia), CNPq (Brazil), and CONICET (Argentina)—Observing run ID: GN-2006B-Q-38.

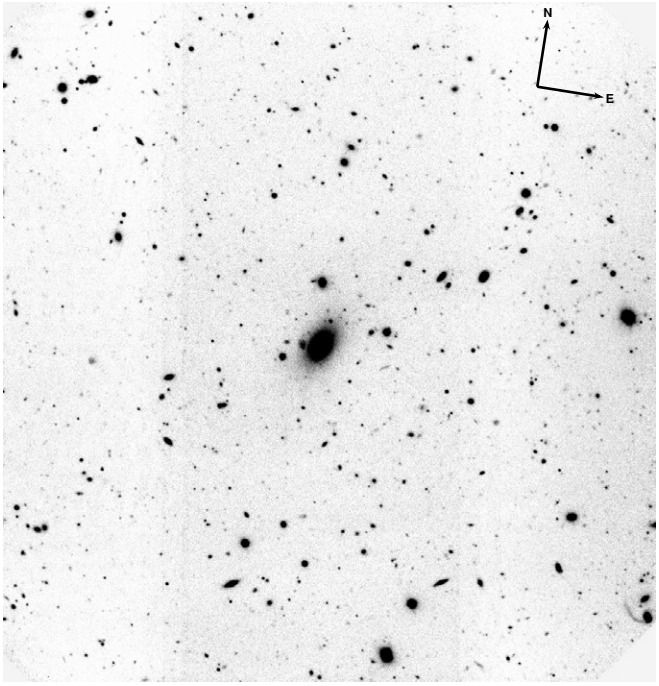

Figure 1. Optical i' image of RX J1340.6+4018. The field of view is 5.6 arcmin on a side, or $\sim 980\,h_{70}^{-1}$ kpc at the object redshift. The field orientation is shown in the upper right corner of the figure.

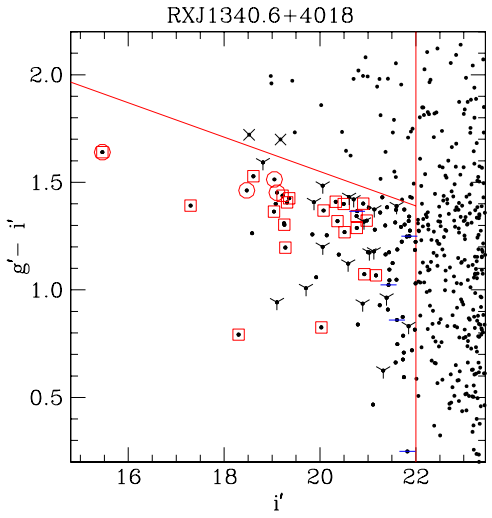

Figure 2. Color–magnitude diagram of the galaxies in the RX J1340.6+4018 field. Points marked with squares (members), "Y" (nonmembers), and "–" (with spectra but no redshift) represent the galaxies observed spectroscopically by us with GMOS-N. The circles and "X" represent, respectively, members and nonmembers published by Jones et al. (2000). The inclined line indicates the upper limit for the cluster red-sequence which we adopted when selecting the spectroscopic targets, whereas the vertical line is the limit in magnitude up to which we chose objects for spectroscopic follow-up ($i' = 22$ mag).

(A color version of this figure is available in the online journal.)

(Ponman et al. 1994), D'Onghia & Lake (2004) claimed that FGs may pose a severe problem for the cold dark matter (CDM) models, since they did not have as much substructure as expected for such massive systems. On the other hand, Sales et al. (2007) using the millennium simulation found that the luminosity functions of three FGs, including RX J1340.6+4018, are not inconsistent with ΛCDM predictions, although the authors stress that the current sample of FGs with reliable luminosity functions is still poor. Reinforcing this idea, Zibetti et al. (2009), who recently estimated the substructure function from photometric data for six fossil systems (also including RX J1340.6+4018), finds that these systems are consistent with normal clusters and with numerical simulations as well. New measurements and improvements in the determination of luminosity functions for these systems is of paramount importance to determine their origin. Here, we revise the luminosity function of the system RX J1340.6+4018, which is considered the prototype fossil group (Ponman et al. 1994).

In Section 2, we describe the optical and X-ray data we used in this work. In Section 3, we present the results we obtain using the optical data. In Section 4, the results obtained from the X-ray data as well as the result of a test for the formation scenario of galaxies through cannibalism of L* galaxies are presented. Section 5 summarizes and discusses our findings. Throughout this paper, we adopt, unless explicitly mentioned otherwise, a cosmology with $H_0 = 70\,\mathrm{km\,s^{-1}\,Mpc^{-1}}$, $\Omega_0 = 0.3$, and $\Omega_\Lambda = 0.7$, so that $1'' \approx 2.9$ kpc at the cluster distance ($z = 0.172$, see Section 3.1).

2. OBSERVATIONS AND DATA REDUCTION

The imaging and multi-slit spectroscopic observations of the group RX J1340.6+4018 were done with the GMOS instrument, mounted on the Gemini North telescope, on 2006 May 2 and 2006 June 22, respectively (see Sections 2.1 and 2.2 below). The X-ray study was based on archival *Chandra* data, as described in Section 2.3.

2.1. Optical Imaging

The imaging consisted of 3 × 200 s exposures in each of the two filters from the Sloan Digital Sky Survey (SDSS) system (Fukugita et al. 1996) g' and i'. The typical FWHM for point sources was $\sim 0\farcs75$ in all images. All observations were performed in photometric conditions. Figure 1 displays the i' image of the system.

The calibration to the standard SDSS system was made using calibration stars observed about one month before the FG observations. No calibration stars were taken in the night of the FG observations, given that the telescope dome had to be closed due to strong winds shortly after the object observation. We confirmed the goodness of the i'-band zero point obtained from the calibration stars by comparing magnitudes measured by us with those from the SDSS database, for 20 galaxies in common, in the magnitude range $i = 18$–20, finding no systematic difference. All observations were processed in a standard way with the Gemini IRAF[5] package version 1.8.

Positions and magnitudes (isophotal and aperture) were obtained for all objects. We estimate that the galaxy catalog is essentially complete down to 24.25 i' magnitude (the peak of the number-count histogram). The SExtractor *stellarity* index (Bertin & Arnouts 1996) was used to separate stars from galaxies. All objects with *stellarity* index $\leqslant 0.8$ were selected as galaxies.

2.2. Optical Spectroscopy

Galaxies for spectroscopic follow-up were selected based on their magnitudes and colors. Figure 2 shows the color–magnitude diagrams for galaxies with $i' \leqslant 23.5$ mag. Objects

[5] IRAF is distributed by NOAO, which is operated by the Association of Universities for Research in Astronomy, Inc., under contract with the National Science Foundation.

Table 1
Spectral Data for Galaxies in the Field of RX J1340.6+4018

(1) Name[a]	(2) R.A. (2000)	(3) Decl. (2000)	(4) i' (AB Mag.)	(5) $g'-i'$	(6) cz (km s^{-1})	(7) R
G29.2+1704	13 40 29.2	40 17 04	20.98	1.32	50379 ± 41	4.1
G18.3+1830	13 40 18.3	40 18 30	19.26	1.30	50455 ± 137	7.0
G30.7+1539	13 40 30.7	40 15 39	18.61	1.53	50679 ± 41	7.2 [c]
G26.4+1811	13 40 26.4	40 18 11	20.76	1.34	50798 ± 57	2.6
G35.9+1826	13 40 35.9	40 18 26	20.33	1.41	50978 ± 39	5.0
G44.2+1902	13 40 44.2	40 19 02	20.36	1.32	51037 ± 60	3.0
G23.6+1817	13 40 23.6	40 18 17	19.31	1.41	51159 ± 48	4.6
G32.5+1612	13 40 32.5	40 16 12	19.36	1.43	51304 ± 46	6.0
G44.5+1637	13 40 44.5	40 16 37	19.04	1.36	51432 ± 100	3.0
G32.4+1533	13 40 32.4	40 15 33	20.77	1.29	51476 ± 38	5.6
G32.6+1910	13 40 32.6	40 19 10	19.22	1.44	51566 ± 30	7.8
G32.8+1740	13 40 32.8	40 17 40	15.46	1.60	51577 ± 39	8.9
G36.5+1843	13 40 36.5	40 18 43	20.50	1.40	51718 ± 64	4.0
G33.1+1753	13 40 33.1	40 17 53	20.90	1.40	51769 ± 84	2.4
G32.7+1934	13 40 32.7	40 19 34	20.92	1.07	51777 ± 64	3.0
G41.1+1558	13 40 41.1	40 15 58	20.07	1.37	51926 ± 37	6.2
G36.0+1604	13 40 36.0	40 16 04	20.51	1.27	52004 ± 36	5.9
G37.6+1517	13 40 37.6	40 15 17	17.30	1.39	52034 ± 32	7.2
G44.3+1612	13 40 44.3	40 16 12	19.28	1.20	52362 ± 18	... [b]
G40.4+1651	13 40 40.4	40 16 51	21.17	1.07	52412 ± 96	... [b]
G20.4+1918	13 40 20.4	40 19 18	20.03	0.83	52417 ± 52	6.8 [c]
G20.3+1924	13 40 20.3	40 19 24	18.30	0.79	52451 ± 27	8.1 [c]
G24.0+1618	13 40 24.0	40 16 18	20.92	1.32	58354 ± 85	2.7
G23.9+1904	13 40 23.9	40 19 04	20.06	1.48	60965 ± 39	6.6
G24.8+1953	13 40 24.8	40 19 53	20.89	0.93	61004 ± 137	... [b]
G40.4+1909	13 40 40.4	40 19 09	18.81	1.59	62707 ± 60	4.5
G18.3+1936	13 40 18.3	40 19 36	21.85	0.83	64905 ± 84	... [b]
G27.1+1642	13 40 27.1	40 16 42	19.71	1.01	66612 ± 44	6.7 [c]
G21.5+1930	13 40 21.5	40 19 30	19.11	0.94	85080 ± 56	4.5 [c]
G40.8+1841	13 40 40.8	40 18 41	20.06	1.20	90732 ± 53	... [b]
G34.4+1906	13 40 34.4	40 19 06	21.32	0.62	108043 ± 18	... [b]
G40.3+1900	13 40 40.3	40 19 00	19.87	1.41	119768 ± 32	... [b]
G19.5+1700	13 40 19.5	40 17 00	21.12	1.18	135990 ± 16	... [b]
G42.5+1705	13 40 42.5	40 17 05	21.60	1.39	145587 ± 39	... [b]
G21.8+1959	13 40 21.8	40 19 59	21.39	0.96	155841 ± 19	... [b]
G27.7+2013	13 40 27.7	40 20 13	20.59	1.12	156092 ± 30	... [b]
G19.9+1732	13 40 19.9	40 17 32	21.13	1.37	163895 ± 48	... [b]
G43.0+1701	13 40 43.0	40 17 01	21.03	1.17	181565 ± 54	... [b]
G26.6+1703	13 40 26.6	40 17 03	20.70	1.42	184426 ± 27	... [b]
G37.8+1818	13 40 37.8	40 18 18	20.61	1.43	191963 ± 27	... [b]

Notes.
[a] The names of the galaxies are based on their 2000 celestial coordinates (R.A. seconds and decl. minutes and seconds). Thus, galaxy Gab.c+defg is located at 13 40 ab.c +40 de fg.
[b] Redshift measured from emission lines.
[c] Spectra with emission lines but with redshift measured from absorption lines.

in the region within and bluer than the red cluster sequence and brighter than $i' = 22$ mag ($M_{i'} < -17.6$, the vertical line in Figure 2) were selected as potential candidates. Galaxies above the red sequence are expected to be in the background, since their colors are redder than the expected colors of elliptical galaxies at the group redshift. The outermost galaxy, which turned out to be a member of the group/cluster, has a distance of 516 h_{70}^{-1} kpc from the X-ray center of RX J1340.6+4018 (which coincides very well with the central galaxy).

Four multi-slit exposures of 2400 s each were obtained through a mask with 1.″0 slits, using the R400 grating, for a final resolution of ∼7–8 Å (as measured from the FWHM of the arc lines), covering approximately the range 4000–8000 Å (depending on the position of each slitlet).

Standard procedures were used to reduce the multi-slit spectra using tasks within the Gemini IRAF package. Wavelength calibration was done using Cu–Ar comparison-lamp exposures before and after the exposures.

Redshifts for galaxies with absorption lines were determined using the cross-correlation technique (Tonry & Davis 1979) as implemented in the package RVSAO (Kurtz & Mink 1998) running under IRAF. The final heliocentric velocities of the galaxies were obtained by cross-correlation with several template spectra. The final errors on the velocities were determined from the dispersion in the velocity estimates using several different galaxy and star templates. In the case of emission-line redshifts, errors were estimated from the dispersions in redshifts obtained using different emission lines. The S/N of the data, measured in the continuum region 6400–6500 Å, ranged from 10 to 32.

Table 1 lists positions, isophotal magnitudes, aperture ($g'-i'$) colors, radial velocities with errors, and the Tonry and Davis

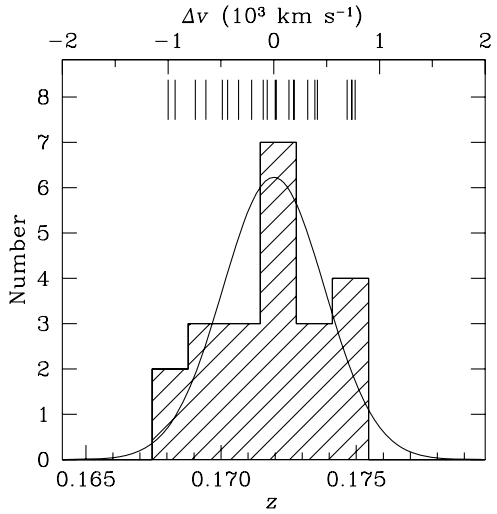

Figure 3. Velocity histogram of RX J1340.6+4018. It shows the distribution of the radial velocities of 22 galaxies in the inner 516 h_{70}^{-1} kpc radius, with redshifts within ±2000 km s^{-1} of the systemic velocity of the group. The sticks on the upper part of the plot show velocities of individual objects. The ROSAT bi-weighted estimator gives a velocity dispersion of $\sigma = 565$ km s^{-1} and a redshift of $\langle z \rangle = 0.1720$, for the sample of 22 objects.

cross-correlation coefficient R for all galaxies with reliable velocity determinations obtained in this study.

2.3. X-Rays

We analyzed *Chandra* archived data of the fossil group RX J1340.6+4018 in order to obtain its temperature and attempt a measurement of elemental abundance ratios. This system was observed by *Chandra* ACIS-S3 in 2002 August for 47.6 ks. The cluster was centered on the S3 chip. The Ciao 3.3.0.1 with CALDB 3.2.4 was used, to screen the data. After correcting for a short flare-like period the resulting exposure time in our analysis was 46.3 ks. A gain map correction was applied together with PHA and pixel randomization. ACIS particle background was cleaned as prescribed for the VFAINT mode. Point sources were extracted and the background used in spectral fits was generated from blank-sky observations using the *acis_bkgrnd_lookup* script.

Here, we show the results of spectral fittings with XSPEC version 11.3.1 (Arnaud 1996) using the APEC and VAPEC thermal emission models. Metal abundances are measured relative to the solar photospheric values of Anders & Grevesse (1989). Galactic photoelectric absorption was incorporated using the WABS model (Morrison & McCammon 1983). Spectral channels were grouped to have at least 20 counts/channel. Energy ranges were restricted to 0.5–8.0 keV. The spectral fitting errors are at the 1σ confidence level, unless stated otherwise. Given that individual abundances require a higher S/N than that observed in the outer regions, we tied oxygen and neon together since they have similar range of yield variation for SN Ia and II. Argon and calcium are not well constrained and were also tied together in the spectral fittings. Fits with these elements untied did not produce significantly different results. For mass yields of SN Ia and SN II, we use the values of Nomoto et al. (1997a, 1997b). SN II yields were calculated integrating over a Salpeter initial mass function (IMF) for a progenitor mass range of 10–50 $M_\odot$.

Table 2
Mass Estimates

(1) Estimator	(2) Mass (10^{14} $M_\odot$)	(3) $M/L_{g'\odot}$ ($M_\odot/L_{g'\odot}$)
Virial	3.23 ± 1.21	330
Projected	4.34 ± 1.42	443
Average	3.10 ± 1.05	316
Median	2.91 ± 1.36	297
Mean value	3.40	347

3. OPTICAL PROPERTIES OF RX J1340.6+4018

3.1. Galaxy Velocity Distribution

Using the heliocentric radial velocities listed in Table 1, we consider as members of RX J1340.6+4018 the 22 galaxies with velocities between 50378 and 52451 km s^{-1} (out of which only five have emission lines). The data were analyzed with the statistical software ROSTAT (Beers et al. 1990), which did not find any large gap in the velocity distribution. In addition, no other data points were found outside a $\pm 3\sigma$ range. Figure 3 shows the velocity histogram for the 22 member galaxies studied by us.

Using the robust bi-weighted estimator of ROSTAT, the following values for the systemic redshift and velocity dispersion were found: $\langle z \rangle = 0.1720 \pm 0.0004$ and $\sigma = 565 \pm 77$ km s^{-1}, respectively. It is in contrast with the earlier result of Khosroshahi et al. (2007) of 419 ± 187 determined for only four galaxies, although not inconsistent, all uncertainties considered. If we characterize the virial radius by the radius within which the interior density is 200 times the critical density (r_{200}), the measured projected velocity dispersion implies a virial radius of $r_{200} = \sqrt{3}\sigma/10H(z) = 1.29 \pm 0.18$ Mpc (Carlberg et al. 1997). The errors are due only to the velocity dispersion determination and do not include the uncertainties implicit in the cited equation (such as departures from a $\rho \propto r^{-2}$ profile at large radii). This value is somewhat higher than that estimated from X-rays (see Section 4), which can be given, as defined in Evrard et al. (1996), by $r_{200} \sim 0.88\sqrt{(kT_{\rm keV})}h_{70}^{-1}$ Mpc $= 1.00 \pm 0.05$ Mpc.

If the optically derived virial radius estimate is taken at face value, it would imply that RX J1340.6+4018 could not be classified "strictly" as a fossil group (in the Jones et al. definition) given that there is one galaxy, G37.6+1517, which is 1.8 mag fainter than the brightest group galaxy in the i' band (1.6 in g'), and which is located at a clustercentric radius of 480 kpc. We note that Santos et al. (2007) has also pointed out that RX J1340.6+4018 did not follow the strict definition of a fossil group.

We determine the dynamical mass of the system by using four different mass estimators, as suggested by Heisler et al. (1985): virial, projected, average, and median mass estimators (see results in Table 2). The adopted center of mass of the system was the brightest cluster galaxy. The errors were calculated by using 1000 bootstrap simulations. Note that the dispersion between the mass values obtained using the several different methods is small compared to the errors in a single measurement. The average of the mass given by the four estimators is 3.4×10^{14} $M_\odot$. We recall that all values are calculated within a radius of 516 h_{70}^{-1} kpc (∼ 40% of the virial radius of the system).

3.2. The Luminosity Function and Mass-to-Light Ratios

We show in Figure 4 the luminosity function of RX J1340.6+4018 (solid circles) for galaxies with spectroscopi-

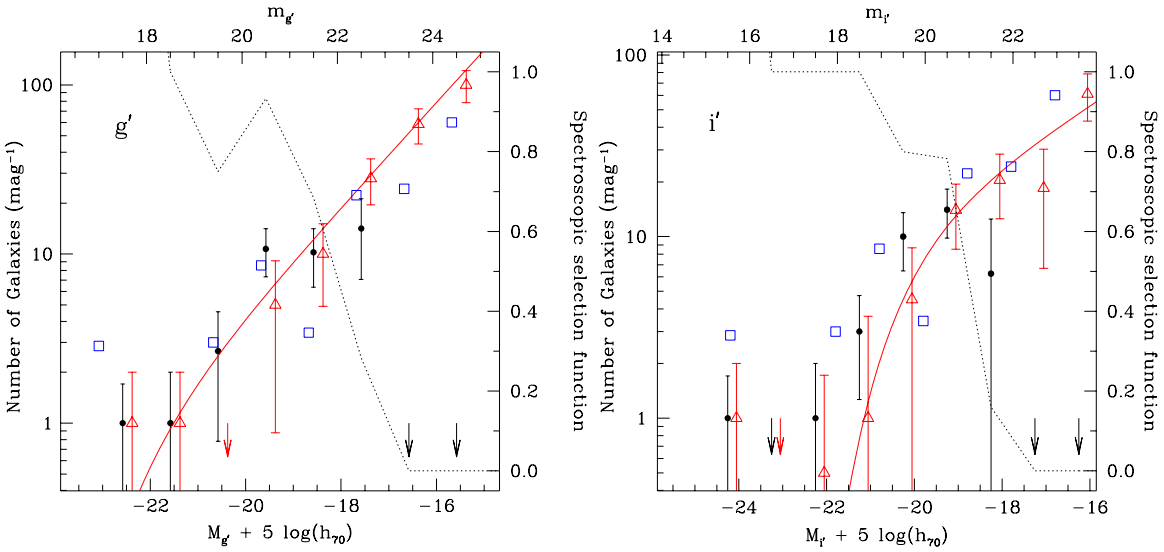

Figure 4. Luminosity functions of RX J1340.6+4018 in the g' and i' bands. The solid circles show the completeness-corrected numbers of spectroscopically confirmed members of RX J1340.6+4018 per 1.0 mag bin in the GMOS field. The error bars are 1σ Poissonian errors. The arrows show bins with number of galaxies less or equal to zero. The dotted line is the selection function of the spectroscopic sample. The open triangles show the photometrically determined luminosity function estimated through number counts and statistical subtraction of the background. The points have been shifted by 0.2 mag (from the center of the bin), for the sake of clarity. The squares represent the luminosity function found for this group by Jones et al. (2000). The continuous lines show the best-fitted Schechter function of the photometric sample. The brightest galaxy of the cluster was not included in the fit. The agreement between the spectroscopically and photometrically determined luminosity functions is good, in the region of overlap.

(A color version of this figure is available in the online journal.)

cally confirmed membership either obtained in this paper (22 galaxies) or given by Jones et al. (2003, three galaxies plus the central one; for the latter we also have a spectrum), corrected for incompleteness. The absolute magnitudes were calculated after correcting the observed magnitudes for Galactic extinction and applying k-corrections. The selection function (number of galaxies with reliable redshifts over the total number of galaxies in a given magnitude bin), also shown in Figure 4, was calculated considering only galaxies bluer than the upper limit of the adopted red cluster sequence.

We have estimated the photometric luminosity function of RX J1340.6+4018 down to the completeness level of our photometric data ($g' = 24.5$ and $i' = 23.5$ mag) by adopting the procedure described in our previous papers (Mendes de Oliveira et al. 2006; Cypriano et al. 2006), where the control fields used for the background subtraction are the ones from Boris et al. (2007). The photometric luminosity functions are shown in Figure 4 as open triangles. They go deeper than the spectroscopic results (solid circles) and they suggest that the number of galaxies keeps increasing at faint magnitudes. It is important to note that, at bright magnitudes, there is no important discrepancy between the luminosity functions calculated using both methods.

In Figure 4, we also overplotted the data from Jones et al. (2000, $R < 400\ h_{50}^{-1}$ kpc $R < 400\ h_{50}^{-1}$ kpc) for the sake of comparison. For that we adopted the colors $g' - R = 0.90$ and $R - i' = 0.54$, which implies an overall $g' - i'$ color of 1.44, which is consistent with our data (see Figure 2) and with the colors of an Sab galaxy at the redshift of 0.17 (Fukugita et al. 1995). By inspection of Figure 4 one can see that Jones et al. and our data sets are consistent with each other, although ours seem to be less noisy, probably due to the use of colors to aid on the background subtraction.

The shape of the luminosity function is very similar in the g' and i'-band diagrams. The faint end of the luminosity function is steeply rising up to our completeness limit. The shape of the photometric luminosity function in the i' band, when fit to a Schechter function in the interval $-22.5 < M_{i'} < -16.5$, is well described by such a function with the following parameters: $M^*_{i'} = -21.3 \pm 1.8$ and $\alpha = -1.6 \pm 0.2$. For the g'-band, the photometric luminosity function is fit in the interval $-21.5 < M_{g'} < -15.5$, and the best fit to a Schechter function is given by the following parameters: $M^*_{g'} = -19.3 \pm 0.9$ and $\alpha = -1.6 \pm 0.2$. Lines indicating the best Schechter luminosity functions fitted are plotted in Figure 4.

We integrated the best-fit Schechter function on the g' band to obtain the total luminosity of the group, assuming that the magnitude of the Sun in the g' band is $M_{g'\odot} = 5.11$ mag.[6] We then added the luminosity of the central galaxy, since this galaxy is not taken into account when fitting the luminosity function. The final result is $9.8 \times 10^{11}\ L_\odot$ on the g' band, where the central galaxy alone is responsible for almost 80% of the entire cluster luminosity budget. This leads to a mass-to-light ratio of 347 $M_\odot/L_{g'\odot}$ (using the mean value for the masses obtained with the four estimators, $3.4 \times 10^{14}\ M_\odot$—see Table 2). Results for the mass-to-light ratio, inside a radius of $516\ h_{70}^{-1}$ kpc ($\sim$40% r_{200}), using different mass estimators, are presented in Table 2.

3.3. Surface Photometry of the BCG

In the upper panel of Figure 5, the azimutally averaged photometric profile of the central galaxy of RX J1340.6+4018 is shown. The surface photometry was performed using the task ELLIPSE in STSDAS/IRAF, which fits ellipses to extended object isophotes. We allowed the ellipticity and position angle of the successive ellipses to change but the center remained fixed. The ellipse fitting was performed only in the deeper i' image. For the g'-band image, the software measured the isophotal levels using the parameters estimated in the i'-band image. There are

[6] Calculated by C. Willmer using the solar spectra: http://www.ucolick.org/~cnaw/sun.html.

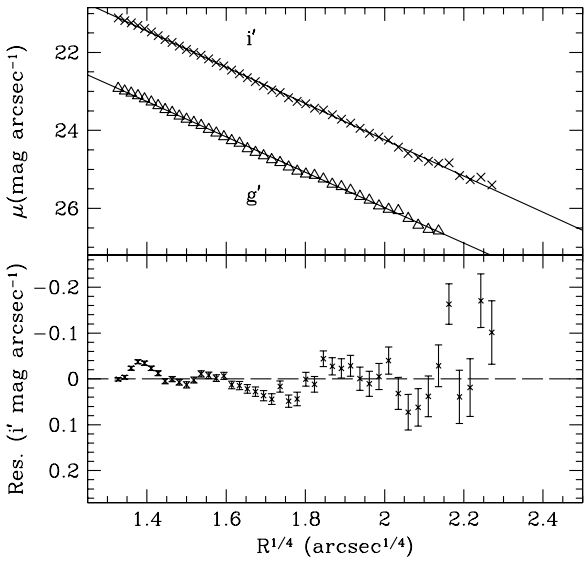

Figure 5. Upper panel: photometric profile of the central galaxy of RX J1340.6+4018. We show the isophotal levels as a function of the semimajor axis to the power 1/4. The solid line is the best fit to the de Vaucoleurs profile in the region where $r > 3.0$ arcsec and $\mu_{i'} = 25.0$ mag arcsec^{-2}. Lower panel: residual between the actual r'-band profile and the de Vaucoleurs profile fit, showing no significant excess that would characterize a cD galaxy.

several small objects within the isophotes of the central galaxy which were masked during the profile-fitting procedure.

We have fitted a $r^{1/4}$-law to the galaxy profile, from well outside the seeing disk (3.″0) to a radius corresponding to $\mu_{i'} = 25.0$ mag arcsec^{-2}. In the lower panel of Figure 5, the residuals (data –$r^{1/4}$-law model) for the i'-band data are shown. There is no light excess over the de Vaucoleurs profile indicating that this galaxy is not a cD.

4. X-RAY PROPERTIES OF RX J1340.6+4018

4.1. ICM Temperature and Abundances

The gas temperature is consistent with a flat profile with a central ($r < 37''$) value of 1.21 ± 0.07 keV and outer value ($112'' > r > 37''$) of 1.31 ± 0.14 keV, consistent within the errors with the average value of 1.16 ± 0.08 keV determined by Khosroshahi et al. (2007). If a cold core is present, it is very mild and not seen with the current statistics. The iron abundance is consistent with a flat profile, but shows marginal signs of a central enhancement. Its central value is 0.29 ± 0.09 Solar and in the outer regions we can only set an upper limit of 0.2 Solar. The measured value of the intracluster gas X-ray luminosity from 0.5 to 10 keV of RX J1340.6+4018 is ∼2.3 × 10^{43} h_{50}^{-2} erg s^{-1}. According to the relations for groups and clusters from Mahdavi & Geller (2001), we find that for a system with this X-ray luminosity we would expect a velocity dispersion of about $\sigma = 425$ km s^{-1}, in good agreement with our direct measurement, given the high scattering in the L_X–σ relation (±240 km s^{-1}).

4.2. Central Abundance Ratios and Fossil Group Formation Models

The isolation of the central galaxy in FGs and the correlation between the FG's X-ray and central galaxy's optical luminosities suggest that the formation process of these systems involve the merging of central bright galaxies due to dynamical friction. Given the timescales for dynamical friction, it was originally suggested that FGs have an earlier formation epoch than regular groups (e.g., Ponman et al. 1994). This is also in agreement with predictions of the concentration parameters and magnitude differences of the two brightest galaxies in FGs from numerical simulations (Wechsler et al. 2002; D'onghia et al. 2005). However, the cooling time of FGs is observed to be significantly below the Hubble time (e.g., RX J1416.4+2315, ESO 3060170, Sun et al. (2004); NGC 6482, Khosroshahi et al. 2004, 2006), but they typically *lack cooling cores*, in disagreement with what one would expect for an old undisturbed system. This is a notable difference from regular rich groups, which often show cooling cores (e.g., Finoguenov & Ponman 1999), even in spite of strong active galactic nucleus (AGN) activity.

To try to solve this apparent contradiction it is desirable to have other independent formation age indicators. Elemental abundances measured in the central regions of FGs can be used as such (Dupke et al. 2009). The general idea is based on the fact that different metal enrichment mechanisms contaminate the intragroup medium with different relative ejecta dominance and are more intense at different cluster locations and in different timescales. For example, protogalactic winds are dominated mostly by SN II and produce an early more distributed background of SN II ejecta throughout the group/cluster, while ram pressure stripping happens continuously throughout the cluster's history and creates a more concentrated SN Ia contamination, given its dependence on the ambient density.

If the group has an earlier origin and has been undisturbed for a long time, the above-mentioned enrichment processes will develop a radial chemical gradient in such a way as to increase the central Fe mass fraction dominance from SN Ia, which is observed in rich groups and clusters of galaxies (e.g., Dupke 1998; Dupke & White 2000a, 2000b; Allen et al. 2001; Finoguenov et al. 2000; Dupke & Arnaud 2001). If the mergers are "dry," i.e., involving gasless galaxies, an older system should have a higher SN Ia central enhancement than a younger system. This central SN Ia enhancement has not been observed yet in any FG. In fact, most FGs seem to have an inverted trend of reduced central SN Ia dominance (Dupke et al. 2009), suggesting that, without fine tuning, the difference between FGs and regular groups is not due to age but to the type of merger that created the central galaxy. Gas-rich galaxy mergers presumably would be accompanied by SN II powered winds, diluting the SN Ia central dominance.

In order to compare the enrichment distribution, we selected two regions for spectral analysis. The first corresponds to the typical cooling radius, where the cooling time is less than the Hubble time (assumed as ∼100 kpc or 10% of r_{200}, which is determined according to $r_{200} \sim 0.88\sqrt{(kT_{\rm keV})}h_{70}^{-1}$ Mpc) and is denoted $r_{\rm cool}$. The second region is an annulus going from the border of $r_{\rm cool}$ to ∼320 kpc, denominated outer in Table 3. A central circular region with 5 kpc radius was excluded to account for possible AGN contamination. Even though the current observation does not allow us to determine variations of the abundance of different α-elements significantly, there seems to be an overall tendency for the abundance of the α-elements silicon, sulfur, oxygen, and magnesium to decline toward the central regions. The results are shown in Table 3 and suggest a gradient in the supernovae type enrichment dominance, unlike that of other FGs (Dupke et al. 2009), but similar to that found in rich groups and poor clusters. The number of counts is very small for the analysis of individual ratios, so that we can only analyze an ensemble of abundance ratios. The error-weighted average of the abundance ratios O/Fe, Si/Fe, S/Fe, and Mg/Fe

Table 3
Individual Elemental Abundance Profiles[a]

Element	Inner r_{cool}[b]	Outer[b]
O	$0.0^{+0.15}_{-0.0}$[c]	$0.4^{+2.0}_{-0.40}$
Mg	$0.41^{+0.46}_{-0.36}$	$1.55^{+1.95}_{-0.85}$
Si	$0.26^{+0.29}_{-0.22}$	$0.44^{+0.96}_{-0.34}$
S	$0.0^{+0.26}_{-0.0}$	$1.78^{+3.72}_{-1.78}$
Fe	$0.29^{+0.10}_{-0.09}$	$0.0^{+0.2}_{-0.0}$

Notes.
[a] Abundances are measured relative to the solar photospheric values of Anders & Grevesse (1989), in which Fe/H = 4.68×10^{-5} by number.
[b] χ^2_ν for the spectral fittings are 1.16 and 1.52 for 39 and 110 dof for the inner and outer regions, respectively.
[c] Errors are 68% confidence limits.

indicates that the SN Ia Fe mass fraction in the central regions of RX J1340.6+4018 is 91 ± 9% and consistent with ∼0% in the outer parts.

5. DISCUSSION

Here, we summarize our main findings in this optical and X-ray study of RX J1340.6+4018.

1. RX J1340.6+4018 is a cluster-like fossil group at $z = 0.172$, with a velocity dispersion of 565 km s^{-1} and a mass of $\sim 3.4 \times 10^{14}\ M_\odot$ within 516 h_{70}^{-1} kpc (about 40% of its virial radius). Thus, the prototype FG is indeed a cluster, not a group.
2. We find a steep faint-end for the galaxy luminosity function of the cluster (with $\alpha = -1.6 \pm 0.2$), which is consistent with the data points published by Jones et al. (2000) and also with the Virgo and Coma luminosity functions. We conclude that there is little room for claims that the low-mass (faint) end of fossil groups is essentially different from that of clusters such as Virgo (D'Onghia & Lake 2004). Thus, they do not pose a problem for CDM models (see also Zibetti et al. 2009).
3. The brightest object of RX J1340.6+4018 is not a cD galaxy. Its surface brightness profile follows closely a de Vaucouleurs law out to 2.5 effective radii.
4. The X-ray analysis of the elemental abundance ratio profiles indicates that the Fe mass fraction in the central region is dominated by SN Ia contamination, similar to other groups and poor clusters of galaxies. This suggests that either the merger which originated the central galaxy was "dry" (the galaxies involved in this process were gas poor), or the group has been formed at early epochs.
5. RX J1340.6+4018 does not constitute a low-density environment. Like RX J1552.2+2013 and RX J1416.4+2315, this object is a galaxy cluster with a large magnitude gap in the bright end. The fairly high X-ray emission, the large fraction of elliptical galaxies (most of the bright galaxies in Figure 1 are early-types), the radial velocity distribution (Figure 3), as well as the lack of obvious substructures, imply a high degree of virialization for RX J1340.6+4018.

Fossil groups have, by definition, a lack of bright galaxies because of the selection criteria used to catalog them. The bright-end of the luminosity function of these systems is then known to be unusual, with too few L^* galaxies. At the faint-end, not much has been known so far, but a scenario seems to be emerging that the massive FGs have steep luminosity functions with exception of perhaps RX J1552.2+2013, for which we just reach the magnitude of the dwarf upturn (the point where the curve goes from being giant-dominated to dwarf-dominated). For the particular case studied here, of RX J1340.6+4018, the faint end of its luminosity function is very steep ($\alpha = -1.6 \pm 0.2$) but, within the errors, it is similar to that of other galaxy clusters of comparable masses. For example, for the 2dF and RASS–SDSS clusters, $\alpha \simeq -1.3$ in the blue band (De Propris et al. 2003; Popesso et al. 2005). It is also comparable with the faint-end slope of clusters like Virgo ($\alpha = -1.28 \pm 0.06$, Rines & Geller 2008) and Coma ($\alpha = -1.47 \pm 0.09$, Iglesias-Páramo et al. 2003). It is worth mentioning that the above errors are statistical and, due to cosmic variance, they are probably underestimated.

We found that the central galaxy of RX J1340.6+4018 does not show any light excess over its de Vaucouleurs profile (which would characterize a cD galaxy). So far, only one central galaxy of a FG, that of RX J1552.2+2013, has been classified as a cD (perhaps not coincidentally, it is also the only FG observed to have a declining luminosity function at $\sim M^* + 4$).

The best accepted scenario for the formation of FGs involves the merging of the central bright galaxies. The lack of SN II ejecta dominance in the central regions of RX J1340.6+4018 implies that the mergers that formed the central galaxy were "dry." The overall results are consistent with an early epoch origin for this FG, so that it has been undisturbed for a long time and central replenishment with SN Ia material, through, e.g., ram pressure stripping, has not been affected by secondary SN II winds. The suspected lack of a cooling core in this system is, if this result is confirmed with better data, still an open question. The scenario of fossil group formation may become clearer when more of these groups are studied spectroscopically. Ongoing determinations of the luminosity function for a large sample of fossil groups and the detailed study of the properties of the brightest group members, including the determination of their ages and metal abundances, may also elucidate some of the unsolved problems regarding these systems.

We are grateful to the referee for comments that helped improve the paper and to H. Khosroshahi for communicating velocities for three members of the group, which were used in the determination of the spectroscopic luminosity function. We thank Raimundo Lopes de Oliveira for a careful reading of the manuscript and useful suggestions. We also thank the Gemini staff for obtaining the observations. The authors acknowledge support from the Brazilian agencies FAPESP (projeto temático 06/56213-9), CNPq, and CAPES. Dupke also acknowledges support from NASA grants NNX07AH55G, NAG 5-3247, GO4-5145X, GO5-6139X, NNX06AG23G, NNX07AQ76G, NNX08AB70G, and FAPESP grant 06/05787-5. We made use of the Hyperleda database and the NASA/IPAC Extragalactic Database (NED). The latter is operated by the Jet Propulsion Laboratory, California Institute of Technology, under contract with NASA.

REFERENCES

Anders, E., & Grevesse, N. 1989, GCA, 53, 197
Allen, S. W., Fabian, A. C., Johnstone, R. M., Arnaud, K. A., & Nulsen, P. E. J. 2001, MNRAS, 322, 589
Arnaud, K. A. 1996, in ASP Conf. Ser. 101, Astronomical Data Analysis Software and Systems V, ed. G. H. Jacoby & J. Barnes (San Francisco, CA: ASP), 17
Barnes, J. 1989, Nature, 338, 123
Beers, T. C., Flynn, K., & Gebhardt, K. 1990, AJ, 100, 32
Bertin, E., & Arnouts, S. 1996, A&AS, 117, 393

Boris, N. V., Sodré, L. Jr., Cypriano, E. S., Santos, W. A., de Oliveira, C. M., & West, M. 2007, ApJ, 666, 747
Carlberg, R. G., Yee, H. K. C., & Ellingson, E. 1997, ApJ, 478, 462
Cypriano, E. S., Mendes de Oliveira, C. L., & Sodré, L., Jr. 2006, AJ, 132, 514
Dariush, A., Khosroshahi, H. G., Ponman, T. J., Pearce, F., Raychaudhury, S., & Hartley, W. 2007, MNRAS, 382, 433
De Propris, R., et al. 2003, MNRAS, 342, 725
Díaz-Giménez, E., Muriel, H., & Mendes de Oliveira, C. 2008, A&A, 490, 965
D'Onghia, E., & Lake, G. 2004, ApJ, 612, 628
D'Onghia, E., Sommer-Larsen, J., Romeo, A. D., Burkert, A., Pedersen, K., Portinari, L., & Rasmussen, J. 2005, ApJ, 630, L109
Dupke, R. A. 1998, PhD thesis, Univ. Alabama
Dupke, R. A., & Arnaud, K. 2001, ApJ, 548, 141
Dupke, R. A., Mendes de Oliveira, C., & Sodré, L., Jr. 2009, ApJ, submitted
Dupke, R. A., & White, R. E., III. 2000a, ApJ, 537, 123
Dupke, R. A., & White, R. E. III 2000b, ApJ, 528, 139
Evrard, A. E., Metzler, C. A., & Navarro, J. F. 1996, ApJ, 469, 494
Finoguenov, A., & Ponman, T. J. 1999, MNRAS, 305, 325
Finoguenov, A., et al. 2000, ApJ, 544, 188
Fukugita, M., Ichikawa, T., Gunn, J. E., Doi, M., Shimasaku, K., & Schneider, D. P. 1996, AJ, 111, 1748
Fukugita, M., Shimasaku, K., & Ichikawa, T. 1995, PASP, 107, 945
Heisler, J., Tremaine, S., & Bahcall, J. N. 1985, ApJ, 298, 8
Iglesias-Páramo, J., Boselli, A., Gavazzi, G., Cortese, L., & Vílchez, J. M. 2003, A&A, 397, 421
Jones, L. R., Ponman, T. J., & Forbes, D. A. 2000, MNRAS, 312, 139
Jones, L. R., Ponman, T. J., Horton, A., Babul, A., Ebeling, H., & Burke, D. J. 2003, MNRAS, 343, 627
Khosroshahi, H. G., Jones, L. R., & Ponman, T. J. 2004, MNRAS, 349, 1240
Khosroshahi, H. G., Maughan, B. J., Ponman, T. J., & Jones, L. R. 2006, MNRAS, 369, 1211
Khosroshahi, H. G., Ponman, T. J., & Jones, L. R. 2006, MNRAS, 372, L68
Khosroshahi, H. G., Ponman, T. J., & Jones, L. R. 2007, MNRAS, 377, 595
Kurtz, M. J., & Mink, D. J. 1998, PASP, 110, 934
Mahdavi, A., & Geller, M. J. 2001, ApJ, 554, 129
Mendes de Oliveira, C. L., & Carrasco, E. R. 2007, ApJ, 670, L93
Mendes de Oliveira, C. L., Cypriano, E. S., & Sodré, L., Jr. 2006, AJ, 131, 158
Morrison, R., & McCammon, D. 1983, ApJ, 270, 119
Nomoto, K., Hashimoto, M., Tsujimoto, T., Thielemann, F.-K., Kishimoto, N., Kubo, Y., & Nakasato, N. 1997a, Nucl. Phys. A, 616, 79
Nomoto, K., Iwamoto, K., Nakasato, N., Thielemann, F.-K., Brachwitz, F., Tsujimoto, T., Kubo, Y., & Kishimoto, N. 1997b, Nucl. Phys. A, 621, 467
Ponman, T. J., Allan, D. J., Jones, L. R., Merrifield, M., McHardy, I. M., Lehto, H. J., & Luppino, G. A. 1994, Nature, 369, 462
Ponman, T. J., & Bertram, D. 1993, Nature, 363, 51
Popesso, P., Böhringer, H., Romaniello, M., & Voges, W. 2005, A&A, 433, 415
Rines, K., & Geller, M. J. 2008, AJ, 135, 1837
Sales, L. V., Navarro, J. F., Lambas, D. G., White, S. D. M., & Croton, D. J. 2007, MNRAS, 382, 1901
Sanders, D. B., & Mirabel, I. F. 1996, ARA&A, 34, 749
Santos, W. A., Mendes de Oliveira, C., & Sodré, L., Jr. 2007, AJ, 134, 155
Springel, V., et al. 2005, Nature, 435, 629
Sun, M., Forman, W., Vikhlinin, A., Hornstrup, A., Jones, C., & Murray, S. S. 2004, ApJ, 612, 805
Tonry, J., & Davis, M. 1979, AJ, 84, 1511
von Benda Beckmann, A. M., D'Onghia, E., Gottlöber, S., Hoeft, M., Khalatyan, A., Klypin, A., & Müller, V. 2008, MNRAS, 386, 2345
Wechsler, R. H., Bullock, J. S., Primack, J. R., Kravtsov, A. V., & Dekel, A. 2002, ApJ, 568, 52
Zibetti, S., Pierini, D., & Pratt, G. W. 2009, MNRAS, 392, 525